A Numerical Study of Taylor–Couette Problem for a Rarefied Gas: Effect of Rotation of the Outer Cylinder

Hiroaki Yoshida and Kazuo Aoki

Department of Aeronautics and Astronautics
and Advanced Research Institute of Fluid Science and Engineering,
Graduate School of Engineering, Kyoto University, Kyoto 606-8501, Japan

Abstract. The Taylor–Couette problem for a rarefied gas is studied numerically by the direct simulation Monte Carlo method. The gas is supposed to be contained in an annular domain, bounded by two coaxial rotating cylinders and top and bottom (specularly reflecting) boundaries, and the flow is assumed to be steady and axisymmetric. Special attention is focused on the effect of rotation of the outer cylinder on the type of the induced Taylor-vortex flow. It is shown that different types of flow can coexist stably in a wide range of speeds of rotation of the inner and outer cylinders unless the outer cylinder is rotating fast in the opposite direction to the inner.

INTRODUCTION

The Taylor–Couette problem, the instability of the cylindrical Couette flow and the occurrence of the secondary flow with vortices (Taylor vortex flow) in a fluid between two coaxial rotating cylinders, is a classical problem in fluid dynamics (e.g., Ref. [1, 2, 3]). However, the study of this problem for a rarefied gas started much later, and several numerical studies with different emphases [4, 5, 6, 7, 8] have been carried out by using the direct simulation Monte Carlo (DSMC) method [9]. For instance, the effect of the temperature difference between the two cylinders is investigated in detail in Ref. [8]. Lately, interest has been expanded to more complicated topics, such as the bifurcation of flows when evaporation and condensation take place on the cylinders [10] and the *ghost effect* when the rotation speeds of the cylinders as well as the Knudsen number are infinitesimal [11].

In the previous DSMC studies, the case where only the inner cylinder is rotating is mainly discussed. In the present paper, we investigate the same problem again by the DSMC method, restricting ourselves to the steady and axisymmetric flows. But our attention is focused on systematic understanding of the effect of rotation of the outer cylinder on the type of induced Taylor vortex flow and the parameter range in which different types of flow may exist.

PROBLEM AND ASSUMPTIONS

Let us consider a rarefied gas between two rotating coaxial circular cylinders with a finite length. To describe the problem, we use the cylindrical coordinate system (r, θ, z) with the z axis taken along the common axis of the cylinders. The radius of the inner cylinder is L_I, that of the outer cylinder is L_{II}, and the bottom and top ends of the cylinders are covered with plates located at $z = 0$ and L_z, respectively. Thus, we consider an annular domain $L_I \le r \le L_{II}$, $0 \le \theta < 2\pi$, and $0 \le z \le L_z$. The inner and outer cylinders are rotating around the z-axis at surface velocities V_I and V_{II} in the θ direction, respectively, and both cylinders are kept at a common temperature T_0. We investigate the steady behavior of the gas numerically on the basis of kinetic theory under the following assumptions: (i) the flow field is axisymmetric; (ii) the gas molecules are hard spheres; (iii) the gas molecules undergo diffuse reflection on the surface of the cylinders ($r = L_I$ and L_{II}) and specular reflection on the bottom and top boundaries ($z = 0$ and L_z). In the present study, special attention is focused on the effect of the rotation of the outer cylinder on the flow patterns.

Since the basic equations are essentially the same as those of Ref. [8] and the space is limited in the present proceedings, we omit them for brevity. We only note that, by introducing appropriate dimensionless variables, one finds that the present problem is characterized by the following five dimensionless parameters: L_{II}/L_I, L_z/L_I, $V_I/(2RT_0)^{1/2}$, $V_{II}/(2RT_0)^{1/2}$, and Kn. Here, Kn$= \ell_0/L_I$ is the Knudsen number, where ℓ_0 is the mean free path of the gas molecules

CP762, *Rarefied Gas Dynamics: 24th International Symposium,* edited by M. Capitelli

Report Documentation Page

Form Approved
OMB No. 0704-0188

1. REPORT DATE	2. REPORT TYPE	3. DATES COVERED
13 JUL 2005	**N/A**	**-**

4. TITLE AND SUBTITLE	5a. CONTRACT NUMBER
A Numerical Study of TaylorCouette Problem for a Rarefied Gas: Effect of Rotation of the Outer Cylinder	5b. GRANT NUMBER
	5c. PROGRAM ELEMENT NUMBER
6. AUTHOR(S)	5d. PROJECT NUMBER
	5e. TASK NUMBER
	5f. WORK UNIT NUMBER
7. PERFORMING ORGANIZATION NAME(S) AND ADDRESS(ES) **Department of Aeronautics and Astronautics and Advanced Research Institute of Fluid Science and Engineering, Graduate School of Engineering, Kyoto University, Kyoto 606-8501, Japan**	8. PERFORMING ORGANIZATION REPORT NUMBER
9. SPONSORING/MONITORING AGENCY NAME(S) AND ADDRESS(ES)	10. SPONSOR/MONITOR'S ACRONYM(S)
	11. SPONSOR/MONITOR'S REPORT NUMBER(S)

12. DISTRIBUTION/AVAILABILITY STATEMENT
Approved for public release, distribution unlimited

13. SUPPLEMENTARY NOTES
See also ADM001792, International Symposium on Rarefied Gas Dynamics (24th) Held in Monopoli (Bari), Italy on 10-16 July 2004.

14. ABSTRACT

15. SUBJECT TERMS

16. SECURITY CLASSIFICATION OF:			17. LIMITATION OF ABSTRACT	18. NUMBER OF PAGES	19a. NAME OF RESPONSIBLE PERSON
a. REPORT **unclassified**	b. ABSTRACT **unclassified**	c. THIS PAGE **unclassified**	**UU**	**6**	

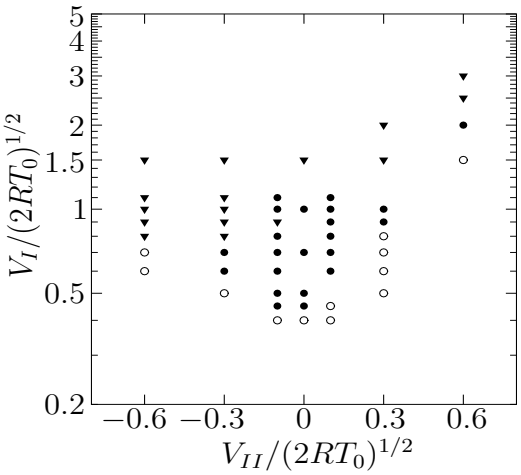

FIGURE 1. Map of the flow patterns in the $(V_{II}/(2RT_0)^{1/2}, V_I/(2RT_0)^{1/2})$ plane for $L_{II}/L_I = 2$, $L_z/L_I = 1$, and $\mathrm{Kn} = 0.01$. The Maxwellian distribution corresponding to the equilibrium state at rest with temperature T_0 and density ρ_{av} is used as the initial condition. The symbols ○, ●, and ▼ indicate that a Couette flow, a single-vortex flow, and a double-vortex flow, respectively, are obtaind at the corresponding points.

in the equilibrium state at rest with temperature T_0 and density ρ_{av} (ρ_{av}: average density of the gas over the annular domain), and R is the gas constant per unit mass.

As the solution method, we use the DSMC method by Bird [9]. As in the usual DSMC computation, we obtain the steady flow field as the long-time limit, pursuing the long-time behavior of the solution of the time-dependent boundary-value problem with an appropriately chosen initial condition.

RESULTS AND DISCUSSIONS

Since the DSMC method is explained in many places, we omit its description for short and show some of the results of computation. More specifically, we restrict ourselves to the case where $L_{II}/L_I = 2$, $L_z/L_I = 1$, and $\mathrm{Kn} = 0.01$ and investigate the effect of rotation speeds $V_I/(2RT_0)^{1/2}$ and $V_{II}/(2RT_0)^{1/2}$ of the cylinders on the flow patterns.

In the actual computation, the square cross section ($L_I \le r \le L_{II}$, $0 \le z \le L_z$ with $L_{II}/L_I = 2$ and $L_z/L_I = 1$) is divided into 120×120 (System I) or 240×240 (System II) square cells of a uniform size; the total number of simulation particles is 144×10^4 (System I) or 576×10^4 (System II); and the time step Δt is $\Delta t = 5 \times 10^{-4} L_I (2RT_0)^{-1/2} = 5 \times 10^{-4} (2/\sqrt{\pi}) t_0 \mathrm{Kn}^{-1}$, where t_0 is the mean free time corresponding to ℓ_0. Except Fig. 7, the results presented in this paper are based on System I.

First we perform computation, taking the Maxwellian distribution corresponding to the equilibrium state at rest with temperature T_0 and density ρ_{av} as the initial condition at time $t = 0$. This means that the cylinders start to rotate impulsively at $t = 0$. The computation for various values of $V_I/(2RT_0)^{1/2}$ and $V_{II}/(2RT_0)^{1/2}$ gives three different types of steady flow pattern: an axially uniform flow (Couette flow); a Taylor vortex flow with a single vortex (single-vortex flow); and a Taylor vortex flow with double vortices arranged in the axial direction (double-vortex flow). A map of the flow patterns in the $(V_{II}/(2RT_0)^{1/2}, V_I/(2RT_0)^{1/2})$ plane is shown in Fig. 1. A Couette flow is obtained at the points with ○, a single-vortex flow at the points with ●, and a double-vortex flow at the points with ▼. The negative V_{II} means that the outer cylinder is rotating in the direction opposite to the inner.

For a fixed $V_{II}/(2RT_0)^{1/2}$, a Couette flow is obtained for $V_I/(2RT_0)^{1/2}$ smaller than a critical value. The critical value is smallest at around $V_{II}/(2RT_0)^{1/2} = -0.1$ and 0 and increases rapidly with the increase of $V_{II}/(2RT_0)^{1/2}$. When the rotation speed of the outer cylinder is slow, a single-vortex flow is obtained in a rather wide range of $V_I/(2RT_0)^{1/2}$. However, this range shrinks and a double-vortex solution becomes dominant as the rotation speed of the outer cylinder increases, in particular, in the opposite direction.

Figure 1 also shows an isolated double-vortex flow at $V_I/(2RT_0)^{1/2} = 0.9$ in the middle of the range of a single-vortex flow for $V_{II}/(2RT_0)^{1/2} = -0.1$. This fact suggests the possibility of the coexistence of a single- and a double-vortex flow around this parameter range. Our next interest is to investigate whether there is a parameter range in which

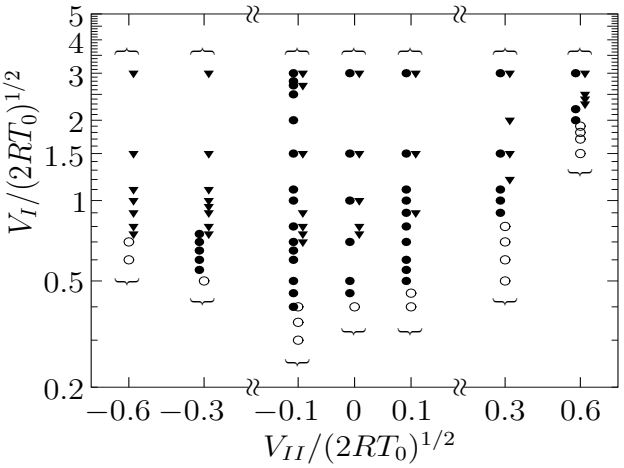

FIGURE 2. Existence range of the steady solutions in the $(V_{II}/(2RT_0)^{1/2}, V_I/(2RT_0)^{1/2})$ plane for $L_{II}/L_I = 2$, $L_z/L_I = 1$, and Kn $= 0.01$. The symbols ○, ●, and ▼ indicate that a Couette flow, a single-vortex flow, and a double-vortex flow, respectively, are obtained at the corresponding points. Here, the symbols stand for the data precisely at $V_{II}/(2RT_0)^{1/2} = -0.6$, -0.3, -0.1, 0, 0.1, 0.3, and 0.6, but ●'s (▼'s) are shifted leftward (rightward) slightly for legibility.

different types of solution coexist stably.

For this purpose, we carry out computation with initial conditions different from the Maxwellian used to obtain the data in Fig. 1. For example, for $V_{II}/(2RT_0)^{1/2} = -0.1$, we take the isolated double-vortex solution at $V_I/(2RT_0)^{1/2} = 0.9$ as the initial condition for a (slightly) smaller value of $V_I/(2RT_0)^{1/2}$, say $V_I/(2RT_0)^{1/2} = 0.8$. If this computation leads to a double-vortex flow, then we use it as the initial condition for a smaller value of $V_I/(2RT_0)^{1/2}$, say $V_I/(2RT_0)^{1/2} = 0.7$. We continue this process until the computation leads to a solution of a different type (i.e., a single-vortex flow or a Couette flow) or a fluctuating state that cannot be regarded as a steady solution. We take a similar procedure for $V_I/(2RT_0)^{1/2}$ larger than 0.9. In this way one can try to extend the range of a stable double-vortex flow for $V_{II}/(2RT_0)^{1/2} = -0.1$ as wide as possible. We carry out the same procedure to extend the range of a stable single-vortex solution, starting from that at the edge of the range in Fig. 1 [i.e., $V_I/(2RT_0)^{1/2} = 0.45$ and 1.1], as well as the range of a stable Couette flow to larger values of $V_I/(2RT_0)^{1/2}$. Essentially the same procedure is carried out for other values of $V_{II}/(2RT_0)^{1/2}$. The result obtained by the above procedure is shown in Fig. 2. The symbols, which have the same meaning as in Fig. 1, indicate the results at $V_{II}/(2RT_0)^{1/2} = -0.6$, -0.3, -0.1, 0, 0.1, 0.3, and 0.6 as in Fig. 1, but ●'s (▼'s) are shifted leftward (rightward) slightly for legibility. In the process of extending the Couette-flow region, we obtained a fluctuating state that cannot be regarded as a steady solution at some points at the edge of the region, but they are not shown in the figure. There is a significant overlap between the region of a single-vortex flow and that of a double-vortex flow when $V_{II}/(2RT_0)^{1/2} \geq -0.1$. For $V_{II}/(2RT_0)^{1/2} = -0.3$, a single-vortex flow is limited to a rather narrow range of intermediate $V_I/(2RT_0)^{1/2}$, and its overlap with the range of a double-vortex flow is small. There is no region of a single-vortex flow for $V_{II}/(2RT_0)^{1/2} = -0.6$ [in this case, we carried out computations for $V_I/(2RT_0)^{1/2} = 0.75$, 8, 9, and 1, using the single-vortex flow at $V_I/(2RT_0)^{1/2} = 0.75$ and $V_{II}/(2RT_0)^{1/2} = -0.3$ as the initial condition and obtained only steady double-vortex flows].

In Figs. 3–5, typical flow patterns of a single- and a double-vortex flow are shown for three points in Fig. 3 where the two types of flow coexist, i.e., $(V_{II}/(2RT_0)^{1/2}, V_I/(2RT_0)^{1/2}) = (0, 1.5)$ in Fig. 3, $(0.6, 3)$ in Fig. 4, and $(-0.3, 0.75)$ in Fig. 5. The panels (a) correspond to the single-vortex flow, and the panels (b) to the double-vortex flow. The arrow indicates the flow velocity vector (v_r, v_z) in the (r, z) plane at its starting point, where v_r and v_z are, respectively, the r and z components of the flow velocity, and the scale of $(v_r^2 + v_z^2)^{1/2}/(2RT_0)^{1/2} = 0.2$ or 0.1 is shown in each figure. The contour line $v_\theta/(2RT_0)^{1/2} = \text{const}$, where v_θ is the θ component of the flow velocity, is also shown in the figures. The obtained double-vortex flows are all symmetric with respect to the plane $z = L_z/2$ and have a clockwise vortex in the upper half $(L_z/2 < z < L_z)$ and a counterclockwise vortex in the lower half $(0 < z < L_z/2)$. In Fig. 5(a), the center of the vortex is as low as that of the lower vortex in Fig. 5(b), and there is almost no flow in the upper part.

A convenient physical quantity that describes the difference of the three types of solution quantitatively would

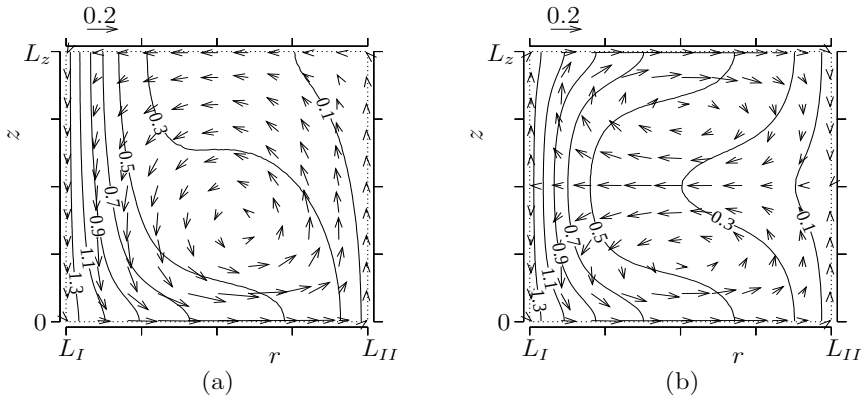

FIGURE 3. Flow field of single- and double-vortex flows for $V_I/(2RT_0)^{1/2} = 1.5$ and $V_{II}/(2RT_0)^{1/2} = 0$ ($L_{II}/L_I = 2$, $L_z/L_I = 1$, Kn $= 0.01$). (a) single-vortex flow, (b) double-vortex flow. The arrow indicates the flow velocity (v_r, v_z) in the (r, z) plane at its starting point, and the scale of $(v_r^2 + v_z^2)^{1/2}/(2RT_0)^{1/2} = 0.2$ is shown in each figure. The contour lines $v_\theta/(2RT_0)^{1/2} = \text{const}$ are also shown in the figure.

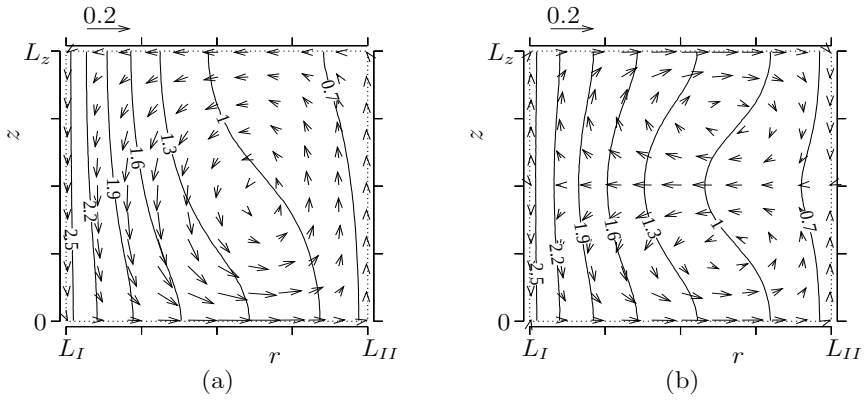

FIGURE 4. Flow field of single- and double-vortex flows for $V_I/(2RT_0)^{1/2} = 3$ and $V_{II}/(2RT_0)^{1/2} = 0.6$ ($L_{II}/L_I = 2$, $L_z/L_I = 1$, Kn $= 0.01$). (a) single-vortex flow, (b) double-vortex flow. See the caption of Fig. 3.

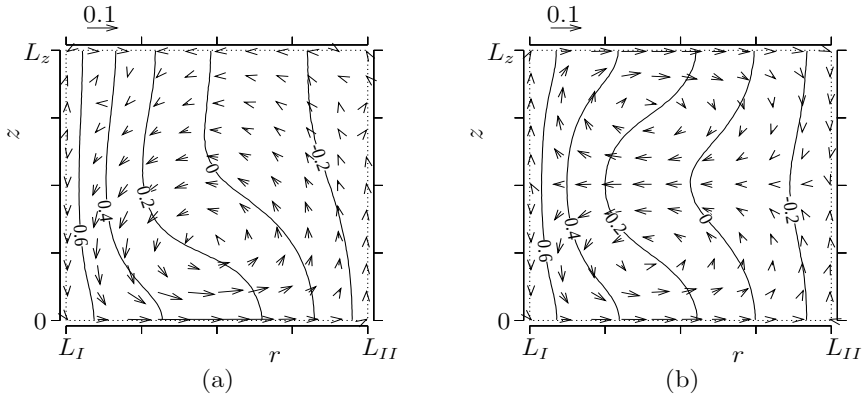

FIGURE 5. Flow field of single- and double-vortex flows for $V_I/(2RT_0)^{1/2} = 0.75$ and $V_{II}/(2RT_0)^{1/2} = -0.3$ ($L_{II}/L_I = 2$, $L_z/L_I = 1$, Kn $= 0.01$). (a) single-vortex flow, (b) double-vortex flow. See the caption of Fig. 3. Here, the scale of $(v_r^2 + v_z^2)^{1/2}/(2RT_0)^{1/2} = 0.1$ is shown in each figure.

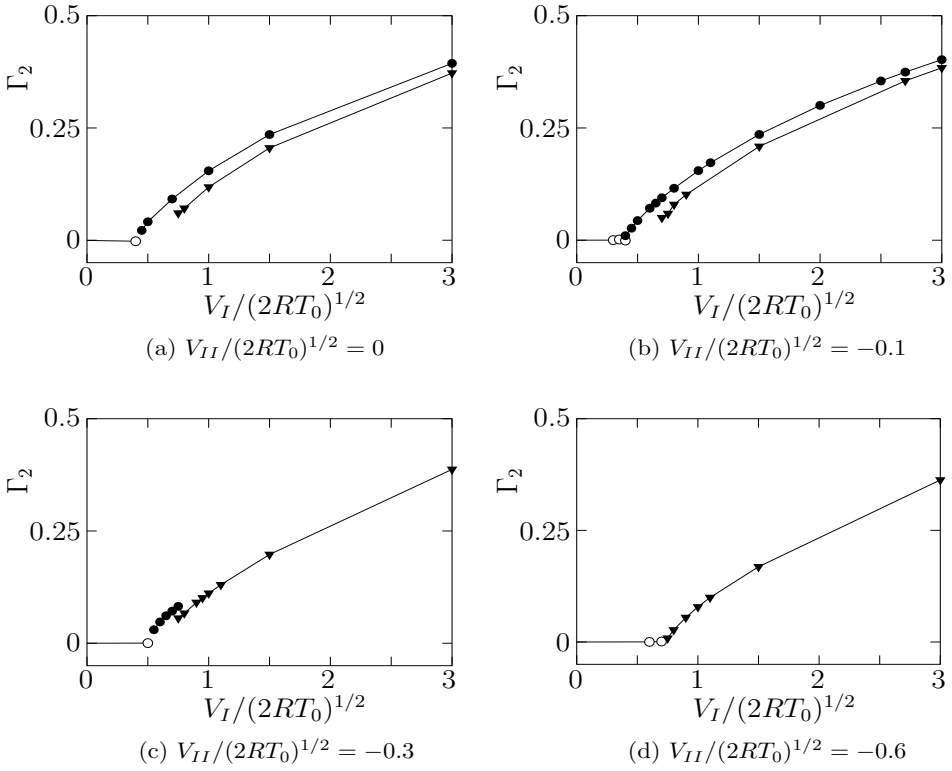

(a) $V_{II}/(2RT_0)^{1/2} = 0$ (b) $V_{II}/(2RT_0)^{1/2} = -0.1$

(c) $V_{II}/(2RT_0)^{1/2} = -0.3$ (d) $V_{II}/(2RT_0)^{1/2} = -0.6$

FIGURE 6. Γ_2 versus $V_I/(2RT_0)^{1/2}$ for typical values of $V_{II}/(2RT_0)^{1/2}$ for $L_{II}/L_I = 2$, $L_z/L_I = 1$, and Kn $= 0.01$. (a) $V_{II}/(2RT_0)^{1/2} = 0$, (b) -0.1, (c) -0.3, and (d) -0.6. The symbols $\circ$, $\bullet$, and $\blacktriangledown$ indicate a Couette flow, a single-vortex flow, and a double-vortex flow, respectively.

be the circulation of the flow velocity vector (v_r, v_z) in the (r, z) plane [8, 10]. We introduce the dimensionless circulation Γ_1 and Γ_2 defined by $\Gamma_m = a_m(2RT_0)^{-1/2}\int_0^{2\pi}[v_z(\hat{r}_m, \hat{z}_m)\cos\phi - v_r(\hat{r}_m, \hat{z}_m)\sin\phi]\mathrm{d}\phi$ $(m = 1, 2)$, where $\hat{r}_m = L_I(1.5 + a_m\cos\phi)$ and $\hat{z}_m = L_I(\alpha_m + a_m\sin\phi)$ with $a_1 = 0.3$, $\alpha_1 = 0.5$ and $a_2 = 0.23$, $\alpha_2 = 0.25$; that is, Γ_1 (Γ_2) is the circulation along the circle of radius $0.3L_I$ ($0.23L_I$) centered at $(r, z) = (1.5, 0.5)L_I$ [$(r, z) = (1.5, 0.25)L_I$]. Note that $\Gamma_1 = \Gamma_2 = 0$ for a Couette flow, and $\Gamma_1 = 0$ for a double-vortex flow that is symmetric with respect to the middle plane $z = L_z/2$. Therefore, to distinguish the three types of flow at the same time, it is more convenient to use Γ_2. Figure 6 shows Γ_2 versus $V_I/(2RT_0)^{1/2}$ for $V_{II}/(2RT_0)^{1/2} = 0$, -0.1, -0.3, and -0.6. Here, the values of Γ_2 are calculated using the averages of the solution over 5×10^5 time steps after the steady state is established. From Fig. 6, it is likely that both branches, the branch of a single-vortex flow and that of a double-vortex flow, bifurcate from the Couette flow. However, the double-vortex flow may be unstable for the values of $V_I/(2RT_0)^{1/2}$ near the bifurcation point except the case of high-speed opposite rotation, $V_{II}/(2RT_0)^{1/2} = -0.6$. In contrast, the single-vortex flow may lose stability rapidly from the large values of $V_I/(2RT_0)^{1/2}$ when the rotation speed of the outer cylinder increases in the opposite direction, and it may become unstable for all $V_I/(2RT_0)^{1/2}$ at $V_{II}/(2RT_0)^{1/2} = -0.6$.

Figures 2 and 6(b) show that both of a Couette flow and a single-vortex flow exist stably at $V_I/(2RT_0)^{1/2} = 0.4$ in the case of $V_{II}/(2RT_0)^{1/2} = -0.1$. Such an overlap between the range of a Couette flow and a single-vortex flow is not observed for other $V_{II}/(2RT_0)^{1/2}$. Therefore, we have to verify whether there is such a small overlap or not more carefully. As pointed out with a concrete example in [10], it is generally very difficult to obtain reliable results for sensitive problems, such as the bifurcation of flows and the onset of instability, by the DSMC method unless one uses very fine cells and an extremely large number of simulation particles. Thus, we investigate more closely the behavior of the solution in the vicinity of the point where a Couette flow and a single-vortex flow coexist, i.e., $V_I/(2RT_0)^{1/2} = 0.4$ and $V_{II}/(2RT_0)^{1/2} = -0.1$, using a larger computational system (System II). The result of the computation is shown in Fig. 7(a), where Γ_1 rather than Γ_2 is shown because the difference between a Couette flow and a single-vortex flow is

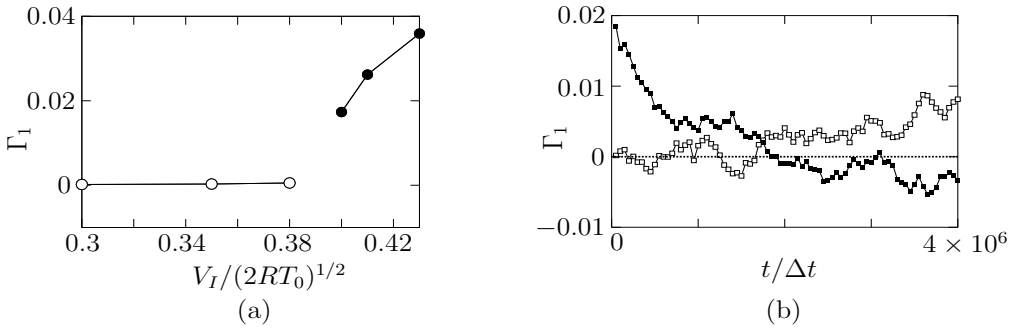

FIGURE 7. Results obtained with System II for $V_{II}/(2RT_0)^{1/2} = -0.1$ ($L_{II}/L_I = 2$, $L_z/L_I = 1$, Kn $= 0.01$). (a) Γ_1 vs $V_I/(2RT_0)^{1/2}$. The symbols ○ and ● indicate a Couette flow and a single-vortex flow, respectively. (b) Time evolution of Γ_1 for $V_I/(2RT_0)^{1/2} = 0.39$. The symbol ■ indicates the data with the initial condition of the single-vortex solution obtained for $V_I/(2RT_0)^{1/2} = 0.40$, and □ those with the initial condition of the artificial Couette flow.

clearer for Γ_1. The single-vortex solution at $V_I/(2RT_0)^{1/2} = 0.43$ was obtained by the impulsive rotation as in Fig. 1. Then we extended the branch of a single-vortex flow down to $V_I/(2RT_0)^{1/2} = 0.40$ by the same way as the construction of Fig. 2. However, the computation for $V_I/(2RT_0)^{1/2} = 0.39$ using the single-vortex solution at $V_I/(2RT_0)^{1/2} = 0.40$ as the initial condition did not converge to any clear steady solution. The time evolution of the circulation Γ_1 in this case is shown by the symbol ■ in Fig. 7(b). On the other hand, the Couette flows at $V_I/(2RT_0)^{1/2} = 0.3$, 0.35, and 0.38 were obtained from special initial conditions explained in the following. One can always obtain the axially uniform Couette flow by imposing the uniformity in the z direction. By using such a solution in each layer of the cells piling up in the z direction, we can generate an artificial Couette flow without constraint of axial uniformity. Such flows generated for $V_I/(2RT_0)^{1/2} = 0.3$, 0.35, and 0.38 were used as the initial conditions for corresponding cases. It is likely that one can obtain a stable Couette flow more easily from this type of initial condition. However, such a computation at $V_I/(2RT_0)^{1/2} = 0.39$ did not lead to any clear steady flow. The time evolution of Γ_1 in this case is shown by the symbol □ in Fig. 7(b). In Fig. 7(b), the Γ_1 at $t/\Delta t = n$ is calculated with v_r and v_z averaged over $t/\Delta t = (n - 5 \times 10^4 + 1) \sim n$. By the way, in all the flows that we judged as Couette flows, Γ_1 and Γ_2 at large time exhibit rather high-frequency oscillations around zero as time goes on . From Fig. 7, we may conclude that there is no overlap between the range of a Couette flow and that of a single-vortex flow and that the overlap observed in Fig. 6(b) is a false behavior caused by the insufficiency of the computational system (System I).

ACKNOWLEDGMENTS

This work is supported by the Grants-in-Aid for Scientific Research (Nos. 14350047 and 16001161) from JSPS and by the Center of Excellence for Research and Education on Complex Functional Mechanical Systems.

REFERENCES

1. Taylor, G. I., *Phil. Trans. R. Soc. London Ser. A*, **223**, 289-343 (1923).
2. Chandrasekhar, S., *Hydrodynamic and Hydromagnetic Stability*, Oxford University Press, London, 1961.
3. Chossat, P., and Iooss, G., *The Couette-Taylor Problem*, Springer-Verlag, New York, 1994.
4. Stefanov, S., and Cercignani, C., *J. Fluid Mech.*, **256**, 199-213 (1993).
5. Reichelmann, D., and Nanbu, K., *Phys. Fluids A*, **5**, 2585-2587 (1993).
6. Usami, M., in *Rarefied Gas Dynamics*, edited by Harvey, J. and Lord, G., Oxford University Press, Oxford, 1995, pp. 389-395.
7. Bird, G. A., in *Rarefied Gas Dynamics*, edited by Shen, C., Peking University Press, Beijing, 1997, pp. 149-154.
8. Aoki, K., Sone, Y., and Yoshimoto, M., in *Rarefied Gas Dynamics*, edited by Brun, R., Campargue, R., Gatignol, R., and Lengrand, J.-C., Cépaduès-Éditions, Toulouse, 1999, Vol. 2, pp. 109-116.
9. Bird, G. A., *Molecular Gas Dynamics*, Oxford University Press, Oxford, 1976; *Molecular Gas Dynamics and the Direct Simulation of Gas Flows*, Oxford University Press, Oxford, 1994.
10. Sone, Y., Handa, M., and Sugimoto, H., *Transp. Theory Stat. Phys.*, **31**, 299-332 (2002).
11. Sone, Y., Handa, M., and Doi, T., *Phys. Fluids*, **15**, 2903-2915 (2003).